JVST B
Journal of Vacuum Science & Technology B

Fabrication of three-dimensional opal nanolattices using template-directed colloidal assembly

Cite as: J. Vac. Sci. Technol. B **40**, 062803 (2022); https://doi.org/10.1116/6.0002112
Submitted: 27 July 2022 • Accepted: 20 September 2022 • Published Online: 09 November 2022

Vijay Anirudh Premnath, I.-Te Chen, Kun-Chieh Chien, et al.

JVST B
Journal of Vacuum Science & Technology B

ARTICLE

avs.scitation.org/journal/jvb

Fabrication of three-dimensional opal nanolattices using template-directed colloidal assembly

Cite as: J. Vac. Sci. Technol. B 40, 062803 (2022); doi: 10.1116/6.0002112
Submitted: 27 July 2022 · Accepted: 20 September 2022 ·
Published Online: 9 November 2022

Vijay Anirudh Premnath, I.-Te Chen, Kun-Chieh Chien, and Chih-Hao Chang[a)]

AFFILIATIONS

Walker Department of Mechanical Engineering, The University of Texas at Austin, Austin 78712

Note: This paper is part of the Special Topic Collection: Papers from the 65th International Conference on Electron, Ion, And Photon Beam Technology and Nanofabrication (EIPBN 2022).

[a)]**Electronic mail:** chichang@utexas.edu

ABSTRACT

Three-dimensional (3D) nanostructures play a crucial role in nanophotonics, lasers, and optical systems. This article reports on the fabrication of 3D nanostructures consisting of opal structures that are spatially aligned to an array of holes defined in the photoresist. The proposed method uses colloidal lithography to pattern a hexagonal array of holes, which are then used to direct the subsequent 3D assembly of colloidal particles. This approach allows the 3D opal structures to be aligned with the 2D array of holes, which can enhance spatial-phase coherence and reduce defects. The polymer patterns can be used as a sacrificial template for atomic layer deposition and create free-standing nanolattices. The final structure consists of a combination of nanolattice, upon which controlled deposition of opal structures is achieved. These structures result in nanostructured materials with high porosity, which is essential to create low-index materials for nanophotonics. A thick layer of titanium oxide with high refractive index is deposited over nanolattices to demonstrate the mechanical stability of underlying structures. These nanolattice structures with precisely controlled height can serve as a low-index layer and can find applications in Bragg reflectors, nanophotonics, and optical multilayers.

I. INTRODUCTION

The advent of nanofabrication has opened tremendous opportunities for acoustics, photonics, aerospace, and microelectronics industries, enabling materials with superior properties to bulk materials and exhibiting unexpected scaling laws.[1–13] These structures have desirable properties such as a greater strength to stiffness ratio, high deformability, and recovery rates, which make them attractive materials for emerging technologies including battery and flexible electronics. It is noted that porous structures with irregular architectures tend to have poor mechanical properties compared to hierarchical and periodic structures, where specific strength increases with the corresponding reduction in the density of lattice architectures.[3–6,14] 3D nanostructures can also have reduced thermal conductivity and can be used for critical applications such as a heat insulator in integrated circuits and battery nanoelectrodes.[5] Porous nanostructures also enhance heat transfer since they promote radiative energy transfer, which is faster.[6–8] 3D nanostructures can also be used for battery electrodes due to their high surface area-to-volume ratio. Recent work has demonstrated copper nanorods arranged in a closed packing structure as charge collectors, which improve the performance and lifetime of batteries.[9]

The optical properties of 3D nanostructures can also have interesting properties that depend on the material, geometry, and order of the structures. The manipulation of optical properties can be achieved by varying the size, composition, and geometry of nanolattices. The optical properties are known to have dependencies on the internal electronic structures, and understanding the structure allows varying their properties such as refractive index and, therefore, reflectivity. One example of an optical application is photonic crystals (PhC), which are materials with periodic dielectric profiles along different directions to prevent the propagation of light. There are three types of photonic crystals, classified as 1D, 2D, and 3D crystals, depending on the number of directions along which the dielectric profiles are infused.[10,11] A 1D PhC operates like a Bragg reflector and can achieve 100% reflectance for both TE and TM modes.[12] Optically, the presence of pores in nanostructures can reduce the effective refractive indices to be as close as air.[13–16] This approach overcomes the limitation of traditional bulk

materials, where the lowest refractive index in a solid material is in calcium fluoride and has a value of 1.39.[17] Such low-index materials can improve the performance of photonic elements such as PhC, which depends on having high index contrast. Low-index nanostructures with random porosity can be accomplished using glancing angle deposition[13,15] and solgel processes.[16] Recent work has also shown that periodic nanolattices can have an index as low as 1.025 while having reduced optical scattering.[18] The nanostructures can serve as the low-index medium in Bragg reflectors or 1D PhC to enhance index contrast and achieve perfect reflectivity over a broader wavelength band. Nanostructured materials can also be used to build multilayer photonic structures to have gradient-index profiles where the index is spatially varying for antireflection properties.[19,20]

While 3D nanostructures have significant mechanical, thermal, electrical, and optical applications, the manufacturing of such materials at a large scale is still a significant challenge. Existing nanofabrication processes can be grouped into two categories: Top-down and bottom-up techniques. Top-down techniques generally involve lithography to define the pattern and material deposition or removal from the bulk to achieve nanoscale feature sizes. The bottom-up techniques focus on assembling the nanoscale elements into functional components using interactions between the elements. This process is complicated and has lower throughputs compared to top-down techniques.[21] Bottom-up not only involves the arrangement of elements (such as atoms, particles, DNA, and proteins) into desirable structures but also in the formation of unprompted assembly units into organized structures in the most energy-stable configurations. For instance, the formation of hexagonal closed packed structures by nanosphere arrays in a monolayer is owed to the least surface energy configuration of spheres.[22]

Optical lithography is an important fabrication technique wherein a photosensitive polymer is exposed to light to form the latent image of the desired pattern.[23] A technique using phase shift lithography can be used to pattern 3D structures.[24–26] The setup involves using a periodic phase element (analogous to a photomask), which aids in the formation of a diffraction interference pattern on the photoresist, leading to formation of a volumetric intensity pattern. The angle of diffraction and the patterns formed are governed by the ratio of phase mask period and the wavelength of light used. One facile method to implement phase shift lithography involves the usage of self-assembled nanospheres in hexagonal close-packed structures, which upon UV illumination results in the formation of a 3D intensity pattern.[27] This is based on the principle of the Talbot effect, which provides intensity patterns due to interference between the rays of light, at specified distances along the axial length of the used nanosphere arrays. The distances at which the intensity patterns repeat themselves are called the Talbot distance. This technique avoids the use of actual physical masks, which are replaced by the self-assembly of colloidal particles.[28,29] The 3D photoresist structures can then serve as a sacrificial template to fabricate nanolattices with reduced refractive indices using atomic layer deposition, which has reported a refractive index as low as 1.025.[30] However, in the existing work, the height of the low-index structure is limited by the photoresist thickness and can be limited by the optical absorption of the photoresist.[14] The integration of such low-index nanostructures with solid layers has also not been studied, which can be a critical issue when building photonic multilayers.

In this research, we demonstrate the fabrication of highly porous 3D nanolattices using hollow-core opal structures that are aligned on top of a lithographically defined array of holes. The structures are fabricated by conformally depositing a layer of Al_2O_3 film over a porous resist, patterned using phase shift lithography, creating a porous structure along with multiple layers of hollow opal nanolattices. The thickness of opal nanostructures can be precisely controlled by the number of nanosphere assembly layers, ranging from a single layer to four layers. The inclusion of opal layers allows the direct control of the nanolattice height, which can be designed to control the photonic properties. Following a planarization step, a uniform layer of TiO_2 is deposited to form a capping layer, which facilitates further integration of additional layers. The refractive indices of porous Al_2O_3 nanolattice and TiO_2 layers provide a high refractive index mismatch, which can find applications in building photonic crystals or waveguides.

II. EXPERIMENTAL METHODOLOGY

The schematic of the fabrication process for the proposed 3D nanolattice with hollow opal structures is depicted in Fig. 1. Silicon 100 mm substrates (University Wafer) are spin-coated with 100 nm thickness of an antireflection coating (ARC, Brewer Science i-con-16) and 300 nm thickness of a positive-tone photoresist (Sumitomo Chemical, PFi-88A2). The ARC is applied on the wafer substrate to prevent back reflections from wafer surfaces to reduce the formation of standing waves. Moreover, the ARC layer can also enhance adhesion between the resist layer and the substrate. Polystyrene (PS) nanospheres with 500 nm diameters (Polysciences) are then self-assembled on the photoresist, as shown in Fig. 1(a), forming a hexagonal close-packed array to maintain the least surface energy.[20] The assembled spheres are used as near-field phase shift masks and the samples are exposed to a HeCd UV laser (Kimmon, 325 nm wavelength) with a dose of 110 mJ/cm^2. The exposure of the monolayer of nanospheres generates a volumetric intensity pattern as governed by the Talbot effect,[31] which is recorded in the underlying photoresist. After removing the nanospheres in the ultrasonication bath, the samples are developed for 60 s in a developer solution (Microposit CD-26), resulting in a periodic hole array as shown in Fig. 1(b). During development, additional nanospheres can be coated on photoresist structures, as illustrated in Fig. 1(c). By controlling the concentration of the colloidal solution and assembly process, discrete layers of PS nanospheres can be assembled on the photoresist template.

The 3D photoresist structures and PS nanospheres can then serve as a sacrificial template for atomic layer deposition (ALD). Over this structure, a conformal ALD coating of Al_2O_3 is deposited using a commercial ALD system (Cambridge Savannah TM 200) on the photoresist and PS surfaces, as illustrated in Fig. 1(d). The formation of Al_2O_3 occurs through two self-limiting half-reactions using trimethyl aluminum (TMA) and de-ionized water. The process recipe used is 1/10/1/20 for TMA for the precursor of aluminum/nitrogen purge/de-ionized water for oxide precursor/nitrogen purge, respectively, with all times in seconds, resulting in the formation of 0.1 nm thickness per ALD cycle. The deposition

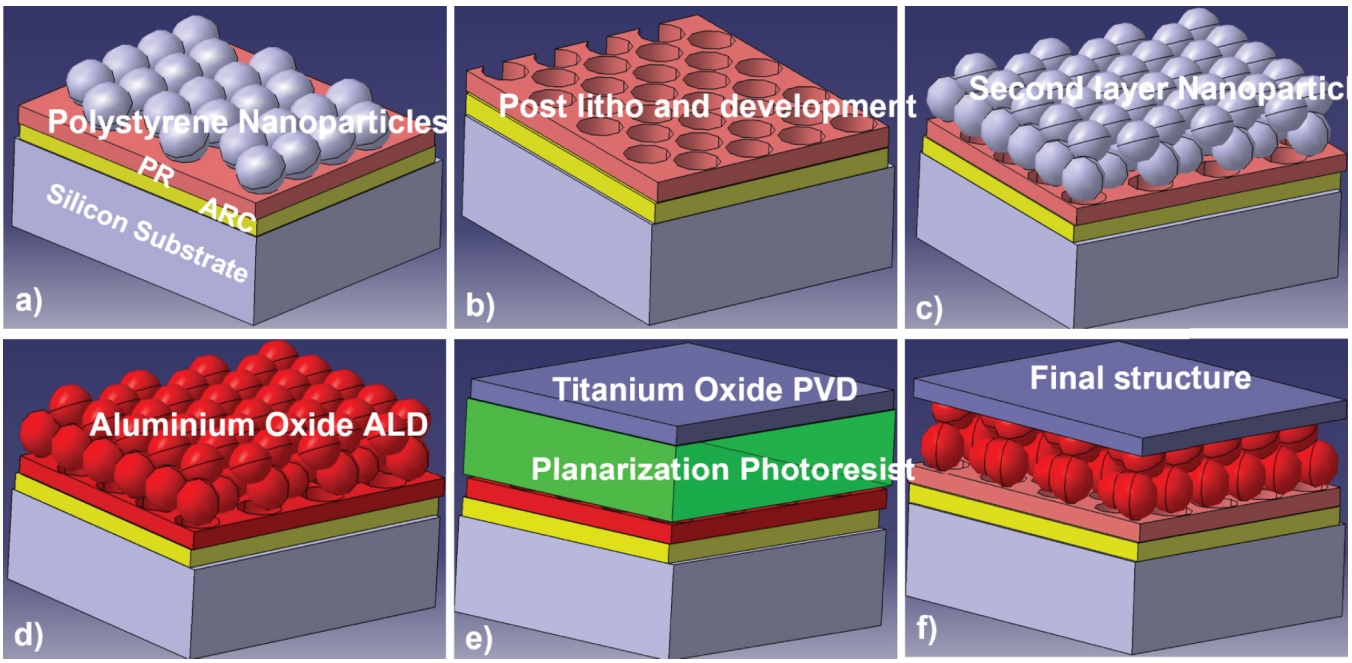

FIG. 1. Fabrication process for a hollow opal nanolattice. (a) Deposition of ARC and PR layers on the silicon substrate over which the nanospheres are transferred manually. (b) Exposure and development of photoresist. (c) Assemble additional PS nanospheres on the photoresist template. (d) Deposit conformal ALD coating on polymer nanostructures. (e) Planarization coating of PR and deposit TiO_2. (f) Removal of PR and buffer layer by temperature treatment.

pressure of 550 m Torr and temperature of 90 °C are used. The conformal coating allows the photoresist to act as a sacrificial template for the nanolattice and was coated to a thickness of 20 nm with 200 cycles.

To planarize the nanolattice to provide a stable base for subsequent layers of coating and to prevent the TiO_2 from depositing into the structure, another layer of PFI 88 resist around 350 nm thickness is spin-coated on the nanolattice to planarize the sample. A solid TiO_2 layer is then deposited using an electron-beam evaporator (Kurt J Lesker PVD-75). The operating voltage at the source is 6000 V, which results in a deposition rate of about 0.26 nm/s. The total thickness of deposition was maintained at 80 nm to provide a thick layer of TiO_2 over the planarized surface as a capping layer, as shown in Fig. 1(e). The structure is baked to a setpoint of 550 °C to remove the photoresist and the PS template, with a ramp-up rate of 1 °C/min, and this is followed by dwelling at the set temperature for 30 min. Finally, the temperature is reduced to 50 °C by cooling it at a rate of 5 °C/min. After the thermal cycle, the remaining 3D structure consists of a stack of nanolattice and hollow opal structures, as illustrated in Fig. 1(f). The TiO_2 capping layer on top of the stack is used to facilitate further integration of an additional material on top of porous nanostructures.

III. RESULTS AND DISCUSSION

The fabrication results for the 2D array of holes as a photoresist template are shown in the scanning electron micrograph (SEM) images depicted in Fig. 2. The sample was exposed to a 100 mJ/cm^2 dose and then the particle was removed using ultrasonication. The top-view SEM image of fabricated structures after development is shown in Fig. 2(a), which shows a uniform distribution of hole array in a hexagonal close-packed (HCP) order. Note the structure has short spatial-phase coherence and forms multiple grain boundaries, which is characteristic of colloidal assembly. The cross section SEM image shown in Fig. 2(b) depicts the uniformity in hole depth of 300 nm as defined by the resist thickness. However, there are a few defects associated with the structure as marked in Fig. 2(a). These include point and assembly defects where missing particles disrupt the neighboring arrangement of HCP structures and contribute to the scattering of fabricated structures. The assembly defects can be attributed to limited uniformity in the sizes of nanospheres, which can have up to 5% variance.[32] Apart from particle defects, there are also impurities and inclusions on the surface of the wafer, though the wafer has been thoroughly cleaned using oxygen plasma, resulting in the formation of voids in the arrangement of particles, and might result in the development of cracks.

Once the 2D array photoresist sample has been fabricated, it can be used as a template to direct the assembly of PS nanospheres. This is achieved by drop casting an aqueous solution of PS nanospheres on the photoresist template and allowing the solution to dry. An initial monolayer is formed by assembling into the holes of the resist template, and additional assembly layers from 2 to 4 layers can be observed by increasing the particle concentration in the solution. This process allows the patterned 2D resist template

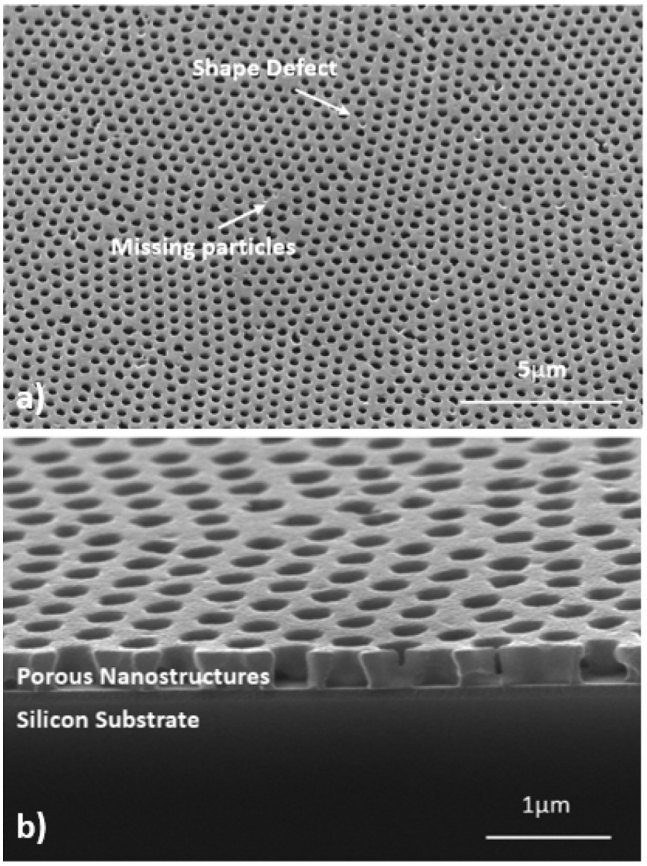

FIG. 2. Cross-sectional SEM images of a fabricated photoresist template. (a) Top view of the patterned photoresist after exposure and development. (b) Side view of the patterned resist exposed from uniform hexagonal closed packing of nanospheres.

and the layers of nanospheres to act as sacrificial layers for ALD to conformally coat the surface. The samples are then planarized in a thick photoresist and coated with a uniform TiO_2 layer and then annealed at 550 °C for 30 min with a small ramp-up rate of 1 °C/min to remove all photoresist and PS. Figures 3(a) and 3(b) depict the schematic of the desired structures and the SEM images of fabricated 3D opal structures. The structure consists of a porous nanostructure around 300 nm thick, which is the result of the conformal ALD coating on the 2D template photoresist structure. The opal structures with hollow cores sit on and are phase aligned to the porous nanostructures, a result of the template-directed assembly process. The height of the opal layer is roughly 500 nm, as governed by a single layer of nanosphere diameter. A uniform layer of TiO_2 with 80 nm thickness can be seen on top, which caps the 3D nanostructures. The fabricated structure creates an interface between the low-index Al_2O_3 opal nanolattices and high-index solid TiO_2 film, thereby enhancing the index mismatch. The presence of more air gaps between the porous and the solid layers, contributed by the void inside the inverse sphere, results in the index mismatch.

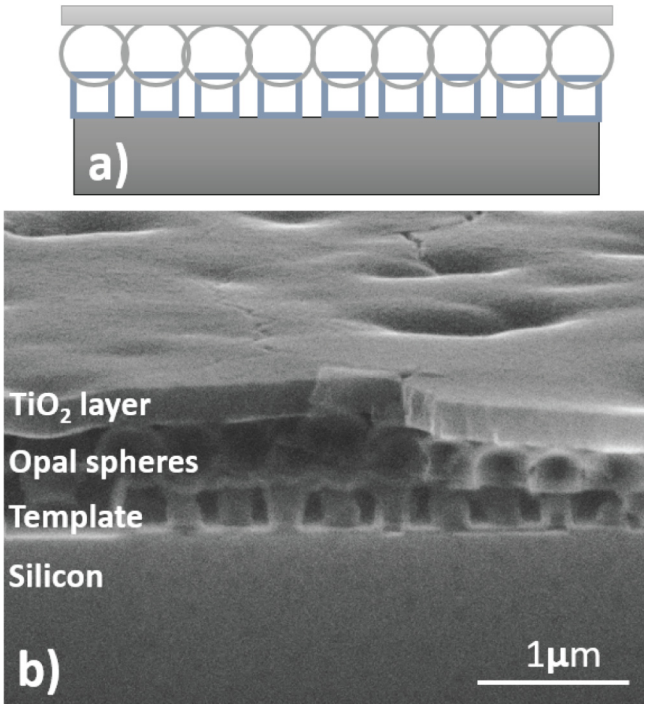

FIG. 3. Illustration of the proposed high porosity opal nanostructure with a capping film to create a high index mismatch interface. The schematic (a) depicts a stack of desired nanostructure consisting of a silicon substrate, porous Al_2O_3 nanostructures, hollow opal nanostructures, and a solid TiO_2 layer. (b) represents the SEM image of the fabricated sample depicting the stacking of the nanostructure.

Taller opal nanostructures can also be fabricated by increasing the number of PS nanosphere assembly layers on the nanostructures template. Figure 4 shows the cross section SEM images of hollow opal structures with increasing height between Al_2O_3 nanolattice and TiO_2 layer. The process can be used to fabricate structures with one to four layers of colloidal assembly. The corresponding thicknesses of the porous 3D nanostructures are 500, 1000, 1500, and 2000 nm for single, two, three, and four assembly layers, respectively. As noted previously in the experimental approach section, the number of layers can be controlled by the concentration of PS nanospheres in the aqueous solution. However, the control of the layer number is not precise in the current drop casting approach, and regions with mixed layer numbers can be observed. The layer count can potentially be further improved by using a layer-by-layer assembly approach, which is the subject of on-going research.

The hollow opal nanostructures can increase the height of the 3D nanostructures, which together with the lattice geometry and ALD thickness can control the effective index of the porous film. Controlling the nanolattice height can change the optical path length within the material, enabling the design of effective photonic crystal reflector over a broader wavelength band. The nanolattice is made of complex 3D nanostructures and is not isotropic, resulting

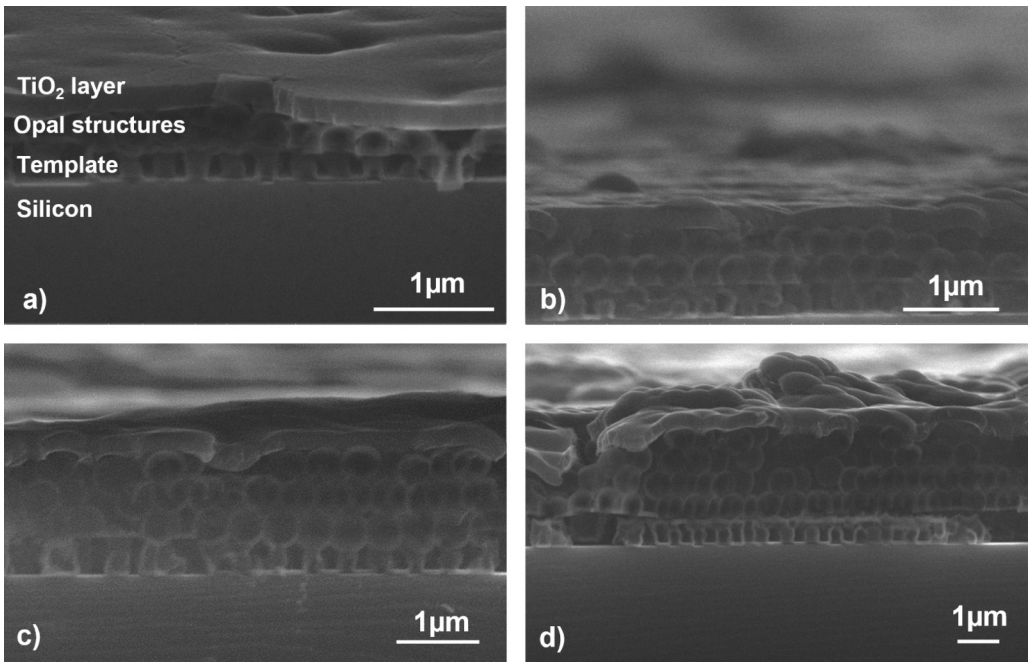

FIG. 4. SEM images of fabricated opal nanostructures containing (a) single, (b) two, (c) three, and (d) four nanosphere assembly layers prior to deposition of the ALD film.

in different optical properties for light polarized in different directions. It is important to note that increasing the number of layers can also result in a corresponding reduction in the mechanical properties due to sagging of the nanolattice layers.

The surface on top of the structures is noted to be more undulated with a corresponding increase in the number of opal layers. This can be attributed to the non-planar surface for the structures with more layers, where assembly defects can be compounded and create rougher topography. These undulations also serve as a region where the refractive index can potentially be spatially varying. It was observed that the bottom layer of nanolattices has deformed dramatically due to the structure collapse, and the nanolattice's thickness becomes shorter than expected. This change in height can be attributed to the transition of the photoresist from the liquid phase to the vapor phase during the polymer evaporation process, which creates surface tension during the thermal cycle. Apart from this, the underlying ARC allows the structure to sink, as it changes to the liquid phase for higher temperatures.[33] The surface undulation can also be contributed to the sagging of the TiO_2 top layer in the voids between porous opal structures. The structures make point contact with the solid layer leading to increased sagging. This is enhanced by thermal variations during electron-beam evaporation and during the baking process to remove resist. Since the energy bandgap of the dielectric reflector scales with the periodically varying refractive index along the thickness direction, the deformation of the nanolattices layer will reduce the periodicity and further reduce the reflectance.

Degradation of mechanical stability in the structures can also be observed, which is found to increase with the increase in the number of layers. This can be attributed to the thermal treatment cycle to remove all the polymers including PR, PS, and ARC. The sacrificial polymer is converted from solid to liquid and then a vapor phase, which can cause the structures to collapse due to surface tension. The evaporation can also be nonuniform in the structure, applying uneven pressure on the walls of porous layers resulting in the collapse. This results in some variation of nanolattice thickness and volume fraction between solid and porous layers. Moreover, the escape of photoresists during postfabrication baking is difficult owing to the number of layers of nanolattices present. This issue can be solved by using a thicker ALD layer for a stronger nanolattice layer.

Another reason is that the ALD does not deposit on the contact points between the spheres, which are in direct contact with no spaces. Therefore, when the PS nanospheres are removed, voids can be observed in the hollow opal nanostructures where the contact points were, as observed in Figs. 3 and 4. The voids can potentially degrade the mechanical properties of the opal structures and cause them to collapse. In the SEM image of the 4-layer opal nanostructure, it is noted that the number of contact points between opal spheres is much more when the number of layers increases. Therefore, the number of voids formed increases with the increase in the number of layers in the fabricated structures.

Another interesting feature observed was the formation of cracks in the uniform layer of TiO_2 film, as shown in Fig. 5, which ranges from macroscale to microscale. The highest crack width was in the order of a few micrometers, and the smallest crack width was about 300 nm wide. This crack can be attributed to two reasons,

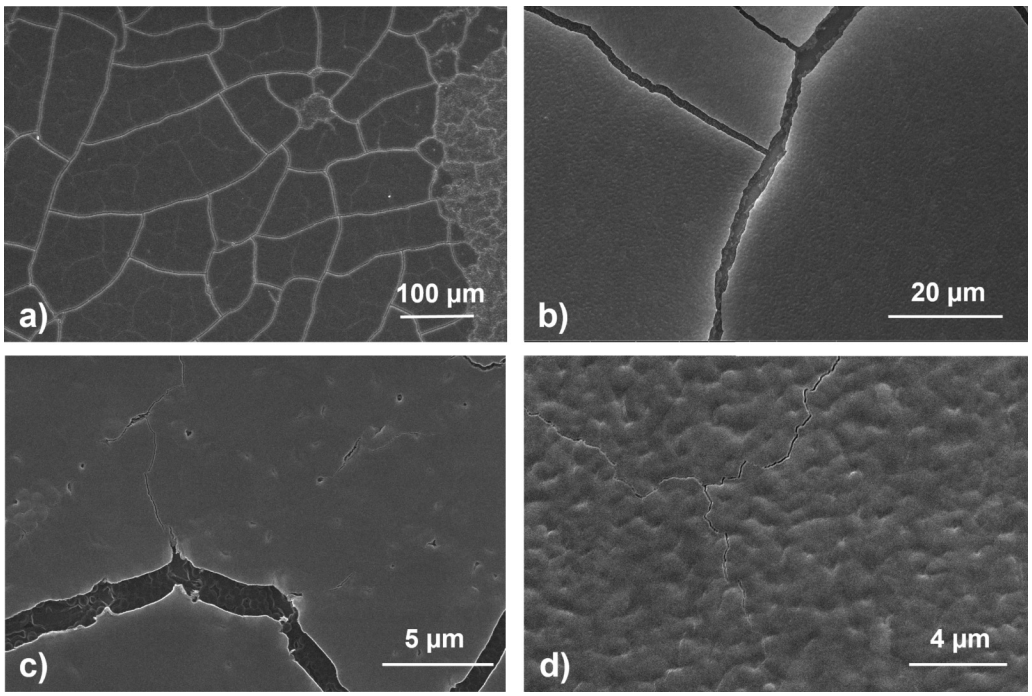

FIG. 5. SEM images of fabricated structures consisting of macro- and microcracks with (a) low magnification of 100 μm scale bar and (b) higher magnification of 20 μm scale bar. (c) Primary microcrack formation over the titanium oxide layer and (d) branched microcracks from primary microcracks that have thickness in the order of 30 nm.

one being the mechanical instability of the structure on top due to height variations during the thermal cycles to remove the polymers. The second reason would be a mismatch in the coefficient of thermal expansion (CTE). The CTE value of TiO_2 is about 8.4×10^{-8} /K, and that of Al_2O_3 is 4.5×10^{-8} /K. The difference results in significant differences in strain during the peak temperature of 550 °C, which can lead to crack formation. The presence of inclusions in the wafer surface, voids, and assembly defects are also minor contributors to crack formation. Though these cracks result in variations in high and low refractive index mismatch, the mechanical stability of the structures is not affected.

IV. CONCLUSIONS

In this research, 3D nanostructures with one, two, three, and four layers of hollow opal structures were fabricated on a 2D nanohole array. The proposed process is fabricated using template-directed assembly of nanospheres, which allows the opal structures to be spatial-phase aligned to the lithographically patterned features. The polymer nanostructures can be used as a sacrificial template for ALD, which results in free-standing Al_2O_3 hollow opal structures after a thermal cycle. The discrete nanostructure layers can be controlled by the nanosphere concentration during assembly, and the total thickness can be controlled from 500 to 2000 nm. Though the increase in number of opal layers leads to taller nanolattice layers that are desirable for photonic applications, there is a reduction in mechanical stability. The structure degradation can be attributed to the thermal process and voids in the ALD structure at the contact points between PS nanospheres. Moreover, it was identified that there are several prominent features on the nanostructures such as macro- and microcracks, and the presence of a defined layer is noted. The demonstrated Al_2O_3 opal structures with a uniform TiO_2 film create an interface with high index contrast, which can be used to improve the performance of multilayer photonic elements.

ACKNOWLEDGMENTS

This work was performed at UT Austin Texas Materials Institute (TMI), Nanomanufacturing System for mobile Computing and Energy Technologies (NASCENT) and Texas Nanofabrication Facilities, which was supported by the National Science Foundation. The work is funded by the NSF under Grant No. CMMI No. 1552424.

AUTHOR DECLARATIONS

Conflict of Interest

The authors have no conflicts to disclose.

Author Contributions

Vijay Anirudh Premnath: Conceptualization (equal); Investigation (equal); Methodology (equal); Writing – original draft (equal); Writing – review & editing (equal). **I.-Te Chen:** Conceptualization

(equal); Data curation (equal); Formal analysis (supporting); Investigation (supporting). **Kun-Chieh Chien:** Formal analysis (equal); Investigation (equal); Methodology (equal); Validation (equal). **Chih-Hao Chang:** Conceptualization (equal); Funding acquisition (equal); Investigation (equal); Project administration (equal); Supervision (equal); Validation (equal); Visualization (equal); Writing – original draft (equal); Writing – review & editing (equal).

DATA AVAILABILITY

The data support the findings of this study are available from the corresponding author upon reasonable request.

REFERENCES

[1]J. Wang, H. L. Duan, Z. P. Huang, and B. L. Karihaloo, Proc. R. Soc. A **462**, 2069 (2006).
[2]S. Wu, Z. Weng, X. Liu, K. W. K. Yeung, and P. K. Chu, Adv. Funct. Mater. **24**, 5464 (2014).
[3]J. Bauer, L. R. Meza, T. A. Schaedler, R. Schwaiger, X. Zheng, and L. Valdevit, Adv. Mater. **29**, 1701850 (2017).
[4]X. Zheng *et al.*, Science **344**, 1373 (2014).
[5]N. G. Dou, R. A. Jagt, C. M. Portela, J. R. Greer, and A. J. Minnich, Nano Lett. **8**, 4755 (2018).
[6]G. P. Zhang, C. Z. Wang, and K. M. Ho, Phys. Lett. A **375**, 1043 (2011).
[7]L. Braginsky, V. Shklover, H. Hofmann, and P. Bowen, Phys. Rev. B **70**, 134201 (2004).
[8]R. Anufriev, J. Maire, and M. Nomura, Phys. Rev. B **93**, 045411 (2016).
[9]Y. Zhao, W. Wan, Y. Chen, R. Erni, C. A. Triana, J. Li, C. K. Mavrokefalos, Y. Zhou, and G. R. Patzke, Adv. Energy Mater. **10**, 2002228 (2020).
[10]E. Yablonovitch, Phys. Rev. Lett. **58**, 2059 (1987).
[11]J. D. Joannopoulos, P. R. Villeneuve, and S. Fan, Nature **386**, 143 (1997).
[12]Y. Fink, J. N. Winn, S. Fan, C. Chen, J. Michel, J. D. Joannopoulos, and E. L. Thomas, Science **282**, 1679 (1998).
[13]J. Q. Xi, J. K. Kim, and E. F. Schubert, Nano Lett. **5**, 1385 (2005).
[14]J.-H. Min, X. A. Zhang, and C. H. Chang, Opt. Express **24**, A276 (2016).
[15]J. Q. Xi, J. K. Kim, E. F. Schubert, D. Ye, T. M. Lu, S. Y. Lin, and J. S. Juneja, Opt. Lett. **31**, 601 (2006).
[16]N. Kawakami, Y. Fukumoto, T. Kinoshita, K. Suzuki, and K. I. Inoue, Jpn. J. Appl. Phys. **39**, L182 (2000).
[17]M. Daimon and A. Masumura, Appl. Opt. **41**, 5272 (2002).
[18]X. A. Zhang, A. Bagal, E. C. Dandley, J. Zhao, C. J. Oldham, B. I. Wu, G. N. Parsons, and C. H. Chang, Adv. Func. Mater. **25**, 6644 (2015).
[19]J. Q. Xi, M. F. Schubert, J. K. Kim, E. F. Schubert, M. Chen, S. Y. Lin, W. Liu, and J. A. Smart, Nat. Photonics **1**, 176 (2007).
[20]I. T. Chen, Z. Dai, D. T. Lee, Y. A. Chen, G. N. Parsons, and C. H. Chang, Adv. Mater. Interfaces **8**, 2100690 (2021).
[21]J. A. Liddle and G. M. Gallatin, ACS Nano **10**, 2995 (2016).
[22]M. H. Yoo, Metall. Mater. Trans. A **12**, 409 (1981).
[23]M. J. Madou, *Fundamentals of Microfabrication: The Science of Miniaturization*, 2nd ed. (CRC, Boca Raton, FL, 2002).
[24]L. Wu, Y. Zhong, C. T. Chan, K. S. Wong, and G. P. Wang, Appl. Phys. Lett. **86**, 241102 (2005).
[25]S. Jeon, J. U. Park, R. Cirelli, S. Yang, C. E. Heitzman, P. V. Braun, P. J. A. Kenis, and J. A. Rogers, Proc. Natl. Acad. Sci. U.S.A. **101**, 12428 (2004).
[26]J. K. Hyun, J. U. Park, E. Kim, L. J. Lauhon, and S. Jeon, Adv. Opt. Mater. **2**, 1213 (2014).
[27]C. H. Chang, L. Tian, W. R. Hesse, H. Gao, H. J. Choi, J. G. Kim, M. Siddiqui, and G. Barbastathis, Nano Lett. **11**, 2533 (2011).
[28]A. Bagal *et al.*, Sci. Rep. **7**, 9145 (2017).
[29]X. A. Zhang, I. T. Chen, and C. H. Chang, Nanotechnology **30**, 352002 (2019).
[30]M. Leskelä and M. Ritala, Thin Solid Films **409**, 138 (2002).
[31]P. Panthong, S. Srisuphaphon, A. Pattanaporkratana, S. Chiangga, and S. Deachapunya, Appl. Opt. **57**, 1657 (2018).
[32]I. T. Chen, E. Schappell, X. Zhang, and C. H. Chang, Microsyst. Nanoeng. **6**, 22 (2020).
[33]H. Duan, J. K. W. Yang, and K. K. Berggren, Nano Micro Small **7**, 2661 (2011).